Simultaneous Concentration and Purification through Gradient Deformation Chromatography

Ajoy Velayudhan and Richard L. Hendrickson
Laboratory of Renewable Resources Engineering, Purdue University, West Lafayette, IN 47907

Michael R. Ladisch
Laboratory of Renewable Resources Engineering, Dept. of Agricultural Engineering, Purdue University, West Lafayette, IN 47907

Mobile-phase additives, commonly used to modulate absorbate retention in gradient elution chromatography, are usually assumed to be either linearly retained or unretained. Previous theoretical work from our laboratory has shown that these modulators, such as salts in ion-exchange and hydrophobic interaction chromatography and organic modifiers in reversed-phase chromatography, can absorb nonlinearly, giving rise to gradient deformation. Consequently, adsorbate peaks that elute in the vicinity of the head of the deformed gradient may exhibit unusual shapes, form shoulders, and/or be concentrated. These effects for a reversed-phase sorbent with aqueous acetonitrile (ACN) as the modulator are verified experimentally. Gradient deformation is demonstrated experimentally and agrees with simultations based on ACN isotherm parameters that are independently determined from batch equilibrium studies using the layer model. Unusual adsorbate peak shapes were found experimentally for single-component injections of phenylalanine, similar to those calculated by the simulations. A binary mixture of tryptophan and phenylalanine is used to demonstrate simultaneous concentration and separation, again in agreement with simulations. The possibility of gradient deformation in ion-exchange and hydrophobic interaction chromatography is discussed.

Introduction

Gradient elution chromatography, in which the mobile phase composition at any point in the chromatographic column is a function of time, is widely used in the analysis and purification of both large and small compounds. Mobile phase additives, or modulators, are used to decrease adsorbate retention and thereby achieve separation (for macromolecules) or decrease separation time (for small molecules). Typical modulators are salts in ion-exchange and hydrophobic interaction chromatography, and organic modifiers such as methanol and aqueous acetonitrile (ACN) in reversed-phase chromatography.

Adsorbate retention in gradient elution has been summarized in Snyder (1980), Snyder and Stadalius (1986), Jandera and Churacek (1985), and Yamamoto et al. (1988), all of whom consider the mobile phase modulator itself to be either linearly retained or unretained. Modulator adsorption, however, is frequently appreciable and can be nonlinear. Then different concentrations of the modulator will move with different velocities, giving rise to gradient deformation. An analogous, but not identical, effect that has been discussed qualitatively in the chromatographic literature is "solvent demixing," which is based on the different velocities with which different components of a multicomponent mobile phase travel. This article is concerned with the consequences of different portions of a single component moving with different velocities, due to nonlinear sorption.

Recent work in our laboratory (Velayudhan and Ladisch, 1991, 1992, 1993) has quantified conditions leading to gradient deformation and described how this could be exploited to obtain simultaneous concentration and purification of moderately retained components. This is achieved by positioning the desired product just behind the head of the gradient, where maximum deformation occurs, so that it will be concentrated while the normal mechanism of gradient elution

Correspondence concerning this article should be addressed to M. R. Ladisch.
Current address of A. Velayudhan: Dept. of Bioresource Engineering, Oregon State University, Corvallis, OR 97331.

causes it to be separated from its impurities. In this article, experimental validation of this concept is presented using reversed-phase chromatography of phenylalanine (Phe) and tryptophan (Trp) in an aqueous ACN gradient as a case study. Batch measurements were carried out to establish the excess isotherm for the ACN–water system on the chosen stationary phase, and the layer model was used to extract the individual isotherm for ACN. A series of gradient elution runs was then carried out, both for Phe alone and for a mixture of Phe and Trp, and shown to give profiles anticipated by the numerical predictions. Gradient deformation based on nonlinear modulator adsorption, as well as simultaneous concentration and separation, is demonstrated.

Materials and Methods

Liquid chromatography system

A Rainin model HPXL (Woburn, MA) gradient system with a flow range of 0–10 mL/min was used, along with a Rheodyne model 7125 injector (Cotati, CA). Eluting amino-acid peaks were detected by UV absorbance at 254 nm using an Isco model V^4 variable wavelength detector (Lincoln, NE). Composition of the ACN–water gradient was measured by a Waters 401 differential refractometer (Milford, MA). Chromatographic effluent histories were recorded on a Linear model 1200 strip chart recorder (Reno, NV). Analytical results were quantitated using a Hewlett-Packard model 3390A reporting integrator (Avondale, PA).

All gradient experiments were run on a 0.78-cm I.D. × 50-cm stainless-steel column capped with stainless-steel end fittings with 10-μ sintered frits (Indianapolis Valve and Fitting, Indianapolis, IN). The reversed-phase adsorbent Amberchrom CG-71sd (Rohm and Haas, Spring House, PA), a polymeric methacrylic material, was used. A mean particle size of 36μ was measured in deionized water using a Malvern Series 2600c Droplet and Particle Sizer (Malvern, England). The same sorbent can be obtained in the 20–50-μ range from Toso Haas (Montgomeryville, PA). The CG-71sd was packed as a slurry at a flow rate of approximately 9 mL/min using a technique developed in our laboratory (Lin et al., 1988). Gradients were formed using 0.45-μ filtered, degassed, deionized water and 99.9% high-performance liquid chromatography (HPLC) grade ACN. The adsorbates used were L-phenylalanine (Serva, Heidelberg, Germany) and L-tryptophan, Sigma Grade (Sigma, St. Louis, MO).

Analytical chromatography runs were carried out on a 4-mm I.D. × 25-cm Rainin Dynamax C-18 column with a particle size of 5 μ and an average pore size of 300 Å. Fractions collected from the gradient runs were analyzed twice, once for ACN and again for the adsorbates (Phe and Trp). ACN samples were run with 0.45-μ filtered, deionized water as the mobile phase at a flow rate of 0.7 mL/min. Peak areas resulting from 20 μL injections were calculated using the recording integrator. Analytical runs for the adsorbates were carried out using a mobile phase of 20% ACN in deionized water at a flow rate of 0.7 mL/min. Sample injections of 20 μL were analyzed on the UV detector at 254 nm.

Isotherm determination

Batch experiments were run in which a fixed amount of the CG-71sd adsorbent in an air-dry state at 16.9% moisture was equilibrated with ACN–water mixtures of different composition. A typical isotherm measurement consisted of weighing 2 g of CG-71sd into a 30-mL Teflon solid-cap vial (Anspec Co., Ann Arbor, MI). A volume of 15 mL of aqueous 40% ACN was added to the vial, which was then capped and placed into a Burrell wrist action shaker (Burrell Co., Pittsburgh, PA). The mixture was gently shaken at room temperature (24°C) for 24 hours. An aliquot of the supernatant was withdrawn and placed in a microcentrifuge tube. Prior to injection, all isotherm samples were centrifuged to remove fine adsorbent particles suspended in solution. The final (equilibrium) ACN concentration was determined by analyzing the supernatant liquid from each batch experiment by HPLC, as described earlier.

The surface molar excess isotherms in Figure 1a were calculated from the batch equilibrium data under the convention that nothing is adsorbed, in moles. Excess isotherm data for ACN-water on octadecyl, reversed-phase silicas with linear or branched C-18 chains, taken from the literature, are also shown in Figure 1a. Remarkable similarity between these C-18 data is evident. The polymeric sorbent used in this study shows significantly greater ACN retention, and the presence of an adsorption azeotrope. Some C-18 silicas also show azeotropy, making it necessary to account for the adsorption of water (the lesser retained component) in constructing an individual isotherm for ACN from the excess isotherm (Slaats et al., 1981). Otherwise, an individual isotherm for ACN that exhibits a maximum would result, which is physically unreasonable.

We therefore use the layer model (Kipling and Tester, 1952; Everett, 1981), in which it is assumed that the stationary phase is always saturated. As the mobile phase composition of the ACN–water mixture changes, so does the stationary phase composition in the saturated layer associated with the stationary phase. The number of layers in this saturated region is found from Rusanov's criteria (Rusanov, 1967): the minimum number of layers is used, provided that the resulting stationary phase mole fractions of ACN and water lie between 0 and 1, and the individual isotherms are monotonic. The individual isotherm for ACN is then obtained as (Everett, 1981)

$$x_i^s = \frac{t_l x_i^l - a_j^0 \Gamma_i^{(n)}}{t_l - \left(a_i^0 - a_j^0\right)\Gamma_i^{(n)}} \tag{1}$$

where t_l is the minimum number of layers consistent with Rusanov's criteria. This is a trial-and-error method: increasing values of t_l are tried, starting with 1, and the first value that satisfies Rusanov's criteria is chosen. The calculation leads to $t_l = 10$.

An alternative direct, that is, noniterative, calculation based on the specific surface area of the adsorbent provides a consistency check. In this method, the areas associated with ACN and water on adsorption can be approximated by a simple packing calculation (Emmett and Brunauer, 1937; Tani and Suzuki, 1989). The theoretical saturation levels of ACN and water are calculated by the method of Schay and Nagy (1961), but allowing for multilayer adsorption. The linear portion of the excess isotherm is extrapolated to the ordinates corresponding to pure ACN and pure water, respectively. Then

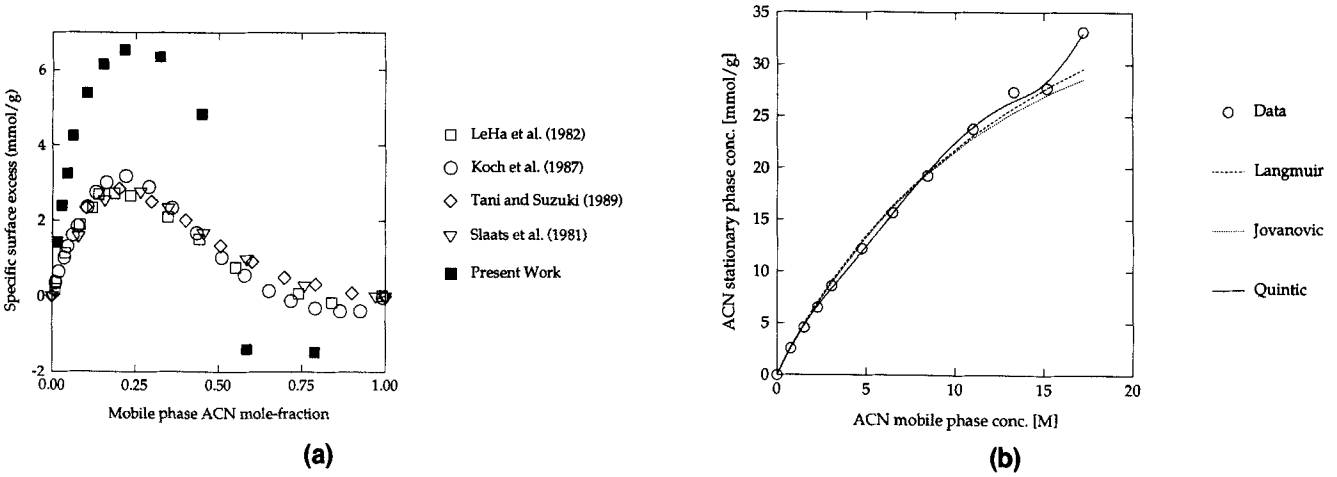

Figure 1. Adsorption of ACN-water on AmberChrom CG-71sd.

(a) Shows the excess isotherm, and (b) the individual isotherm of ACN. (a) Shows several excess isotherms for ACN-water from the literature. LeHa et al. (1982) used a tetradecyldimethyl (branched C-16) chain that they derivatized in-house onto Lichrosorb-SI-100 (Merck, Darmstadt, Germany). Koch et al. (1987) used a commercial octadecyl (linear C-18) chain: Bondapak C-18 (Waters, Milford, MA). Tani and Suzuki (1989) used a homemade octadecyl (linear C-18) chain on Cosmosil 5SL silica (Nacalai Tesgue, Japan). Slaats et al. (1981) used a commercial octadecyl (linear C-18) chain: Lichrosorb RP-18 (Merck, Darmstadt, Germany). Various functional forms, fitted to the data, are also shown in (b). Parameter values for the Langmuir fit are $a_M = 3.50$ mL/g, $b_M = 6.37 \times 10^{-2}$ M^{-1}; for the Jovanovic equation, these are $\Lambda_M = 35.8$ mmol/g and $K_M = 9.29 \times 10^{-2}$ M^{-1}; the quintic equation is $\Sigma a_i C^i$, with $a_0 = 0$, $a_1 = 4.03$, $a_2 = -0.720$, $a_3 = 0.119$, $a_4 = -8.62 \times 10^{-3}$, $a_5 = 2.18 \times 10^{-4}$.

the following independent estimation of the number of layers is available:

$$t_l = \frac{n^s_{ACN} a^0_{ACN} + n^s_{H_2O} a^0_{H_2O}}{A_s}. \tag{2}$$

For the present system, the specific surface area of the sorbent is 500 m^2/g (manufacturer's data), and the adsorption areas are 130 m^2/mmol for ACN and 63 m^2/mmol for water. The saturation concentrations are 27 mmol/g for ACN and 22 mmol/g for water. Substituting these values in Eq. 2, we obtain the following estimate

$$t_l = \frac{4{,}896 \text{ m}^2/\text{g}}{500 \text{ m}^2/\text{g}} = 9.8 \approx 10. \tag{3}$$

This is consistent with our earlier trial-and-error calculation based on Rusanov's criteria. The latter method requires a linear region in the excess isotherm, so that the Schay–Nagy calculation becomes possible. The method is therefore not always applicable, but seems useful for chromatographic systems exhibiting adsorption azeotropy.

The data points for the individual isotherm for ACN, calculated from excess isotherm data as previously described, are shown in Figure 1b. As expected, the individual isotherm is sigmoidal. A quintic polynomial was fitted to the data by nonlinear regression, and Figure 1b shows that the fit is reasonable. Practical uses of ACN gradients, however, involve concentrations well below the extremely high mobile phase concentrations (around 14–15 M) at which the plateau is reached. Consequently, fitting the monotonic data before this plateau to simple isotherm forms such as the Langmuir,

$$q_M = \frac{a_M C_M}{1 + b_M C_M} \tag{4}$$

and the Jovanovic,

$$q_M = \Lambda_M (1 - e^{-K_M C_M}) \tag{5}$$

can be useful. These fits are also shown in Figure 1b, with parameter values for all fits given in the figure legend.

Gradient deformation runs

All gradient runs were carried out on the same Amberchrom CG-71sd methacrylate material used earlier in the batch isotherm studies. The gradient system was described earlier; operating conditions are listed in Table 1. Fractions were collected every 15 s during a gradient run for analysis by HPLC of ACN and adsorbate concentrations, as described earlier.

A linear gradient of 0–100% ACN was run in 40 min. This gradient slope, of 0.47 M/min, was chosen as a representative value for large-scale chromatography, although steeper slopes are frequently used at bench scale. Theory (Velayudhan and Ladisch, 1992) predicts that, under ideal conditions, significant gradient deformation would occur but a true shock wave would not form in the column. Nevertheless, even in the absence of a shock, considerable gradient deformation occurs, as can be seen from the replicate experimental runs

Table 1. Operating Conditions*

Flow rate	1 mL/min
Gradient	0%–100% ACN in 40 min
Temperature	Ambient
Feed volume	2 mL
Feed concentration	0.5 mg/mL (Phe) 0.25 mg/mL (Trp)
Column dimensions	0.78 I.D. × 50 cm length

*Applicable to Figure 2 through 5.

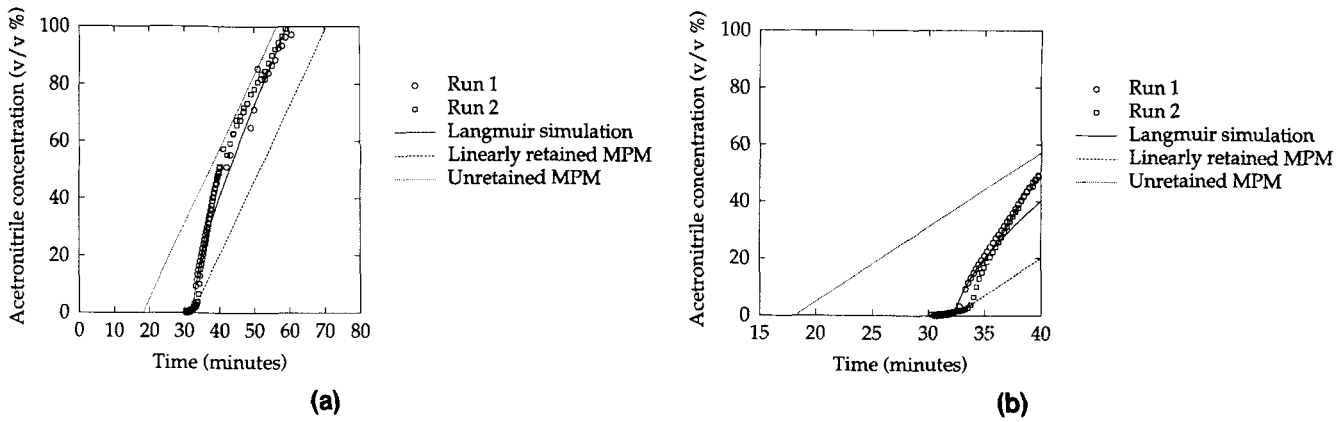

Figure 2. Gradient deformation due to nonlinear modulator adsorption.

Data from 2 runs are shown, as are the predictions based on the present theory as well as the classic unretained and linearly retained theories. Operating conditions are as given in Table 1. (a) Shows the entire run, and (b) is an expanded view of the first 10 min of the gradient.

in Figure 2a. At the head of the gradient, the slope steepens considerably: between 34 and 35 min, the gradient goes from 6.4 to 16.8 M ACN, corresponding to a linear slope of 10.4 M/min; this incipient shock layer has a slope far higher than the initial slope of 0.47 M/min. The corresponding simulation shows a comparable steepening. Since the simulation does not account for bandspreading, it does not capture the shallow region at the head of the experimental gradient. After the experiments were completed, the data suggested that a longer column would be needed for a shock to form under these operating conditions. This is consistent with the previously developed theory, which indicates that a shock would occur just at the outlet of a column that was 16% longer (that is, a 58-cm volume).

The relatively sharp change in slope in the experimental data around 50% v/v ACN could be due to the different extents of swelling undergone by the stationary phase as the mobile phase composition is varied, although this effect is likely to be mitigated in a tightly packed column. Swelling in batch systems was found to increase abruptly at around 50% ACN for the polymeric sorbent. Since the simulation did not incorporate swelling effects, or the possibility of the adsorbent swelling to different degrees as it sees different mobile phase compositions (Marra and Cooney, 1978; Durão et al., 1992), the calculated profile varies smoothly.

Numerical method

A lumped model incorporating overall mass-transfer coefficients is used to describe column dynamics. We first derive it from the following well-known general model for chromatography (Schneider and Smith, 1968; Furusawa et al., 1976; Arnold et al., 1985a).

The mass balance over the interstitial fluid is

$$\epsilon_b \frac{\partial C}{\partial t} + v_{\text{sup}} \frac{\partial C}{\partial x} + (1-\epsilon_b)\frac{\partial \bar{s}}{\partial t} = E\frac{\partial^2 C}{\partial x^2}. \tag{6}$$

The mass balance over the sorbent particles is

$$\epsilon_b \frac{\partial C_p}{\partial t} + \rho_p \frac{\partial q_p}{\partial t} = D_p\left(\frac{\partial^2 C_p}{\partial r^2} + \frac{2}{r}\frac{\partial C_p}{\partial r}\right). \tag{7}$$

These mass balances are coupled by

$$\frac{d\bar{s}}{dt} = \frac{6(1-\epsilon_b)}{d_p} D_p \left.\frac{\partial C_p}{\partial r}\right|_{r=d_p/2} = \frac{6(1-\epsilon_b)}{d_p} k_f (C - C_p|_{r=d_p/2}). \tag{8}$$

Finite sorption kinetics as a first-order process is expressed by

$$\frac{\partial q_p}{\partial t} = \mu_b (K_{\text{ads}} C_p - q_p). \tag{9}$$

Equations 6 through 9, along with standard initial and boundary conditions, account for bandspreading contributions from axial dispersion, film mass transfer, pore diffusion, and finite sorption kinetics. From this general model we first derive the limiting case where only finite sorption kinetics are important; the other sources of bandspreading are considered negligible. Then the following limits are obtained:

$$E \to \infty; \quad \frac{\partial^2 C}{\partial x^2} \to 0; \quad D_i \to \infty; \quad \frac{\partial C_p}{\partial r} \to 0; \quad \frac{\partial^2 C_p}{\partial r^2} \to 0; \quad k_f \to \infty; \quad C_p \to C. \tag{10}$$

Note that the particle concentration $\bar{s}$ is then given by

$$\bar{s} = \epsilon_p C + \rho_p q \tag{11}$$

and the system of Eqs. 6 through 9 reduces to

$$\epsilon_b \frac{\partial C}{\partial t} + v_{\text{sup}} \frac{\partial C}{\partial x} + (1-\epsilon_b)\frac{\partial \bar{s}}{\partial t} = 0 \tag{12}$$

$$\frac{\partial q}{\partial t} = \mu_b (K_{\text{ads}} C - q). \tag{13}$$

Combining Eqs. 11 and 12 results in

$$\{\epsilon_b+(1-\epsilon_b)\epsilon_p\}\frac{\partial C}{\partial t}+\upsilon_{\text{sup}}\frac{\partial C}{\partial x}+(1-\epsilon_b)\rho_p\frac{\partial q}{\partial t}=0. \quad (14)$$

Equations 13 and 14 therefore represent the desired limiting case of finite sorption kinetics as the only source of bandspreading. In order to use this limiting case as a lumped model of the entire bandspreading process, we replace μ_b in Eq. 13 by an overall lumped rate k^0, and choose k^0 so that the bandspreading generated by the general model, Eqs. 6 through 9, will be captured by the lumped model, Eqs. 13 and 14. For this purpose, the retention time and variance of the two models are matched.

The retention time and variance of the general model are available in the literature (Furusawa et al., 1976; Arnold et al., 1985b):

$$t_R=\frac{L}{\upsilon_{\text{sup}}}\{\epsilon_b+(1-\epsilon_b)\epsilon_p+\rho_pK_{\text{ads}}\}+\frac{t_{\text{inj}}}{2} \quad (15)$$

$$\sigma^2=\frac{2L}{\upsilon_{\text{sup}}}\left[\frac{E}{\upsilon_{\text{sup}}^2}\{\epsilon_b+(1-\epsilon_b)\epsilon_p+(1-\epsilon_b)\rho_pK_{\text{ads}}\}^2+(1-\epsilon_b)\right.$$
$$\left.\times\left\{\frac{\rho_pK_{\text{ads}}^2}{\mu_f}+\frac{d_p^2}{6}(\epsilon_p+\rho_pK_{\text{ads}})^2\left(\frac{1}{10D_p}+\frac{1}{k_fd_p}\right)\right\}\right]+\frac{(t_{\text{inj}})^2}{12}. \quad (16)$$

Equations 13 and 14 can be rewritten as

$$\frac{\partial q}{\partial t}+\upsilon_{\text{chrom}}\frac{\partial C}{\partial x}+\phi\frac{\partial q}{\partial t}=0 \quad (17)$$

$$\frac{\partial q}{\partial t}+k^0(K_{\text{ads}}C-q) \quad (18)$$

where

$$\upsilon_{\text{chrom}}\equiv\frac{\upsilon_{\text{sup}}}{\epsilon_b+(1-\epsilon_b)\epsilon_p} \quad (19)$$

and

$$\phi\equiv\frac{(1-\epsilon_b)\rho_p}{\epsilon_b+(1-\epsilon_b)\epsilon_p}. \quad (20)$$

In the form given by Eqs. 17 and 18, the lumped model is identical in form to one given in Ruthven (1984), with υ_{sup} and ϕ replacing υ_{int} and $(1-\epsilon_b)/\epsilon_b$. The physical picture in Ruthven's model is that of external mass transfer being the single source of bandspreading, and consequently his adsorption constant K includes holdup within the pores of the particle, while K_{ads} in Eq. 18 accounts solely for sorbed concentration. Nevertheless, the formal analogy can be used to apply Ruthven's results for retention time and variance to the present lumped model in Eqs. 17 and 18.

The results for retention time (or first moment) is

$$t_R=\frac{L}{\upsilon_{\text{int}}}\left[1+\frac{1-\epsilon_b}{\epsilon_b}\{\epsilon_p+(1-\epsilon_p)K_{\text{vol}}\}\right]+\frac{t_{\text{inj}}}{2}. \quad (21)$$

This can be shown to be equivalent to Eq. 15 by noticing that K_{ads} and K_{vol} have different units and are related through

$$\rho_pK_{\text{ads}}=(1-\epsilon_p)K_{\text{vol}}. \quad (22)$$

Ruthven's result for variance (or second central moment) is

$$\sigma^2=\frac{2L}{\upsilon_{\text{int}}}\frac{1-\epsilon_b}{\epsilon_b}\frac{1}{k^0}\{\epsilon_p+(1-\epsilon_p)K_{\text{vol}}\}+\frac{(t_{\text{inj}})^2}{12}. \quad (23)$$

Equation 23 can be compared to Eq. 16 to obtain the appropriate value of k^0.

Column simulations

The lumped system just given, Eqs. 17 and 18, are now applied to the gradient system with ACN as the modulator and Phe and Trp as the feed components. The governing equations are therefore

$$\frac{\partial C_i}{\partial t}+\upsilon\frac{\partial C_i}{\partial x}+\phi\frac{\partial q_i}{\partial t}=0, \qquad i=\text{ACN,Phe,Trp} \quad (24)$$

$$\frac{\partial q_i}{\partial t}+k_i^0(q_i^*-q_i), \qquad i=\text{Phe,Trp} \quad (25)$$

$$q_{\text{ACN}}^*=\frac{3.50C_{\text{ACN}}}{1+0.0637C_{\text{ACN}}} \quad (26)$$

$$\frac{\phi q_{\text{Phe}}^*}{C_{\text{Phe}}}=(C_{\text{ACN}}+1.07)^{-0.941} \quad (27)$$

$$\frac{\phi q_{\text{Trp}}^*}{C_{\text{Trp}}}=\left(\frac{C_{\text{ACN}}}{2.80}+0.243\right)^{-1.21} \quad (28)$$

Here k_i^0 is the overall mass-transfer coefficient for the ith component, and is calculated as described earlier by comparing Eqs. 16 and 23. Standard correlations and equations from the literature are used to estimate the quantities in Eq. 16. The molecular diffusivity for Phe is available experimentally (Conway, 1952), while that for Trp is calculated from a version of the Wilke-Chang expression due to Snyder and Stadalius (1986). This allows the pore or intraparticle diffusivities to be calculated in the usual way (Satterfield, 1969), accounting for the tortuosity. Wilson and Geankoplis' correlation (1966) is used to estimate the mass-transfer coefficient. Axial dispersion is relatively unimportant for liquid chromatography using small or moderate particles (Ruthven, 1984) and is therefore neglected in Eq. 16. The values of the various parameters are given in Table 2.

Equation 26 represents the Langmuirian form of the ACN individual isotherm calculated earlier. The equilibrium model is used for ACN; hence Eq. 25 does not apply to ACN. The retention of the feed components, as shown in Eqs. 27 and 28, followed usual reversed-phase patterns and were calculated from separate isocratic runs. The adsorbates are assumed to be at concentrations low enough to prevent appreciable interference, and are therefore regarded as moving independently of each other. Single-component isotherm measurements carried out in our laboratory for both Phe and Trp

Table 2. Parameters Used in the Simulations in Figures 2 to 6

Particle diameter $d_p = 60\ \mu m$		
Particle density $\rho_p = 0.38$ g/mL		
Tortuosity $\tau = 4$		
Bed porosity $\epsilon_b = 0.40$		
Particle porosity $\epsilon_p = 0.60$		
Specific surface area $A_s = 500\ m^2/g$		
	Phe	Trp
Film mass-transfer coefficient k_f (cm/s)*	9.47×10^{-3}	9.11×10^{-3}
Pore diffusivity (cm^2/s)†	1.08×10^{-6}	9.48×10^{-7}
Overall lumped mass-transfer coefficient k^0 (min^{-1})‡	35.5	10.2

*From the correlation $Sh = (1.09/\epsilon_b)/(Pe)^{0.33}$.
†From $D_p = (\epsilon_p D_M)/\tau$.
‡From Eq. 11.

were found to be effectively linear in the concentration range of interest.

The column is initially preequilibrated with mobile phase and is free of any feed component. Thus the initial conditions corresponding to the hyperbolic partial differential equation system, Eqs. 24 through 28, are

$$\text{At } t = 0, \quad \begin{cases} C_i = 0, & i = 1,\ldots, N-1 \\ C_N = C_{N,0} \text{ (modulator)} \end{cases} \tag{29}$$

$$\text{At } t = 0, \quad \begin{cases} q_i = 0, & i = 1,\ldots, N-1 \\ q_N = q_N^* = f_N(C_{N,0}). \end{cases} \tag{30}$$

The boundary conditions are

$$\text{At } x = 0, \quad C_i = \begin{cases} C_{i,\text{feed}}, & 0 \le t \le t_{\text{inj}} \\ 0, & t_{\text{inj}} < t \end{cases} \quad i = 1,\ldots,N-1 \tag{31}$$

$$\text{At } x = 0, \quad C_N \begin{cases} C_{N,0}, & 0 \le t \le t_{\text{inj}} \\ C_{N,0} + \alpha(t - t_{\text{inj}}), & t_{\text{inj}} < t. \end{cases} \tag{32}$$

The feed components are injected into the column as a rectangular pulse over a time t_{inj}, the associated mobile phase composition being identical to the preequilibrated state of the column. Then the gradient is fed into the column; here a linear gradient is used, at the inlet, with slope α.

These simple boundary conditions are used instead of the more rigorous Danckwerts' boundary conditions (1953), since Eq. 24 does not account for axial dispersion. (However, as described earlier, the contribution of axial dispersion to adsorbate bandspreading can be incorporated into Eq. 16 when needed.) The hyperbolic system was then solved by the method of characteristics (Acrivos, 1956; Courant and Hilbert, 1962) on a Sun SPARC2 workstation.

Results

Modulator behavior

The predicted effluent ACN history of Figure 2 is bounded by the results from the two classic assumptions—that ACN is unretained, and that it is linearly retained. Under both of these assumptions, since the gradient was linear at the inlet, it remains linear at the outlet. These limiting cases diverge from the experimental results, as expected, since the ACN isotherm is highly nonlinear (cf. Figure 1). An unretained modulator gives rise to a gradient that moves at the mobile phase velocity. Since this is the maximum possible velocity for any component in the given column (neglecting size exclusion effects, and ion exclusion effects in ion-exchange chromatography), the actual gradient cannot emerge from the column earlier than the unretained prediction. Linear retention of the modulator corresponds to the slowest speed the gradient can assume, and therefore represents the upper limit for the actual gradient effluent. The physical basis for these upper and lower bounds is the self-interference (Helfferich and Klein, 1970; DeVault, 1943) of the modulator, and has been described previously (Velayudhan and Ladisch, 1993). In fact, the experimental gradient can be seen to reach these two limiting results at its extremities. At very low ACN concentrations (< 3–4% v/v), the experimental gradient is close to the linearly retained prediction. At high concentrations (beyond 70% v/v), the experimental gradient agrees well with the unretained prediction.

Single-component runs

Adsorbate peak shape is strongly dependent on gradient delay. The effect of delay on peak shape is readily demonstrated, as shown for a series of Phe runs in Figures 3 to 5. In all these figures, the experimental result is shown on the left, and the simulation is shown on the right. In Figure 3a, the part of the Phe peak that emerges before the head of the gradient (before 38 min) elutes isocratically and emerges as a broad front, while the region behind the incipient shock is concentrated to more than twice its feed value. The inlet gradient slope and timing should thus be manipulated to place the desired product just behind the gradient to achieve peak concentration. The formation of a split peak from a single compound is noteworthy, since such a profile might easily be erroneously attributed to an impurity, or to the presence of an on-column reaction. The corresponding simulation, Figure 3b, is for a delay of 4 min, rather than 6 min, since it is for a delay of 4 min that the simulation captures the experimental behavior shown in Figure 3a. This discrepancy is at least partially attributable to the weakly retained impurity present in commercially available Phe. The impurity can be seen more clearly in Figures 4a, and 5a. Since the impurity elutes isocratically in all three figures, it is not the cause of the split peak, which is due to Phe straddling the gradient. The analytical column, on which the capacity factor of Phe as a function of ACN concentration was measured, is only 25 cm long, and did not resolve this impurity from the main Phe peak. Since the dependence of Phe on ACN in the simulation is based on analytical data, the column simulations do not show the impurity. The retention shown in the simulation is therefore an average between the experimental retentions of the weakly retained impurity and the more strongly retained Phe. Thus the Phe in the experiments is more retained than in the simulations, and a given experimental effluent history is only attained by a simulation with a smaller gradient delay.

In Figure 4a, the gradient is delayed by 7 min, one minute

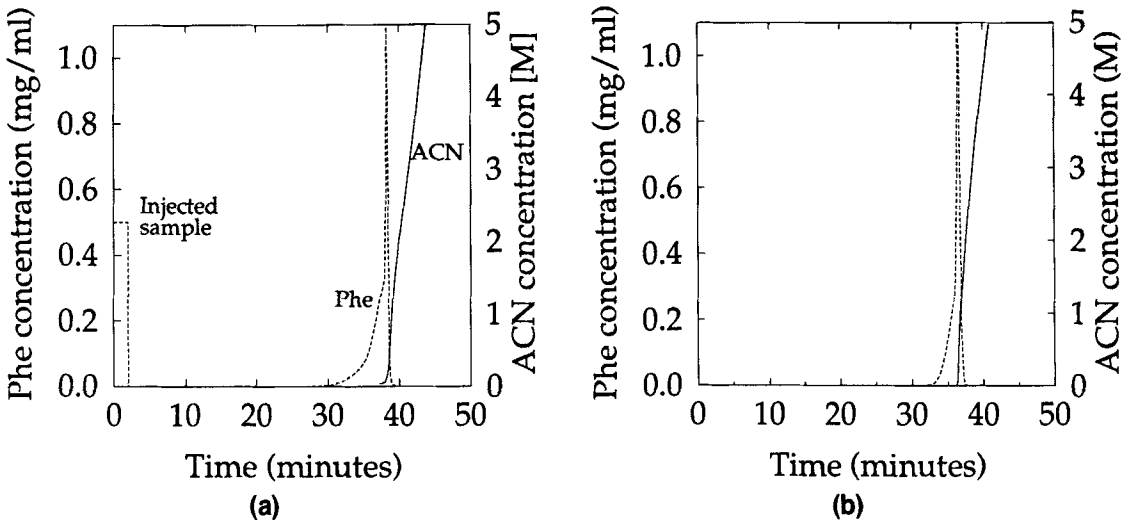

Figure 3. Single-component Phe run.

(a) Shows the experimental result for a delay of 6 min, while (b) shows the simulation for a delay of 4 min (with respect to $t = 0$, when feed introduction begins). Operating conditions as in Table 1.

more than in Figure 3a. This allows more of the Phe to elute before it is overtaken by the gradient. A split peak is again seen, but the concentration effect behind the gradient is less than in part (a), since there is relatively less Phe in this region. The corresponding simulation, Figure 4b, is for a delay of 5 min.

Figure 5a shows a gradient delay of 8 min. Here almost all of the Phe elutes ahead of the gradient; the very small amount of Phe caught by the gradient is seen as a small shoulder starting at 40 min. Since the bulk of the Phe peak elutes isocratically, it is diluted with respect to the feed. The corresponding simulation, Figure 5b, has a delay of 7 min.

Qualitative agreement between simulation and experiments is evident: the same sequence of split peaks is seen, and the Phe found behind the modulator is concentrated. The discrepancy in gradient delay between experiment and corresponding simulation is further described in the Discussion section.

It should be emphasized that there are no fitted parameters in the simulations; all the parameters used are either directly from the manufacturer (such as the specific surface area of the stationary phase) or measured in independent experiments (such as the ACN isotherm, obtained by batch studies, and the adsorbate retention as a function of mobile

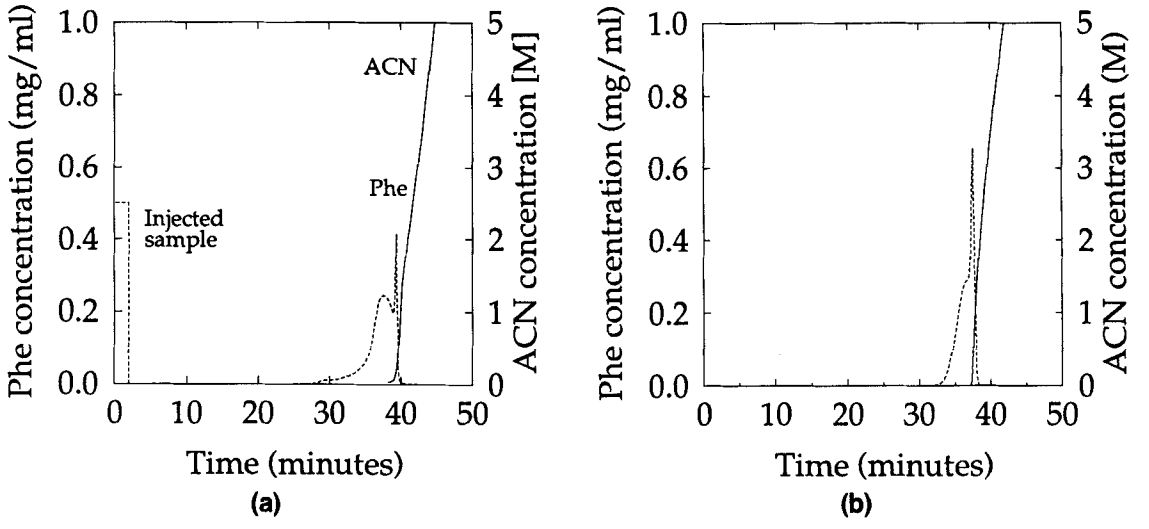

Figure 4. Single-component Phe run.

(a) shows the experimental result for a delay of 7 min, while (b) shows the simulation for a delay of 5 min (with respect to $t = 0$, when feed introduction begins). Operating conditions as in Table 1. Only the gradient in Figure 4a was measured; Figures 3a and 5a show the same gradient shape as in Figure 4a, but with the appropriate delay.

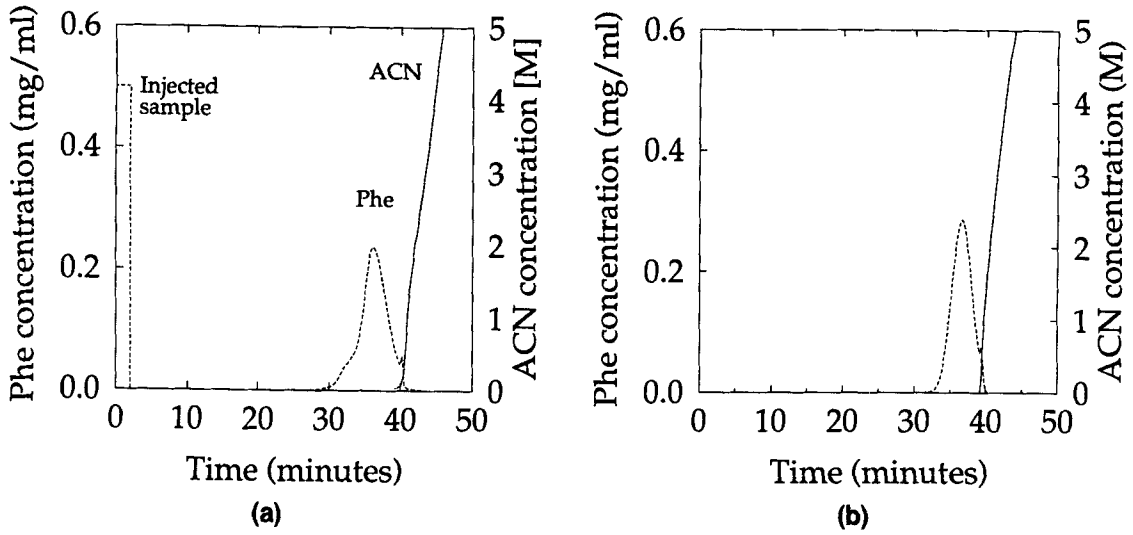

Figure 5. Single-component Phe run.

(a) Shows the experimental result for a delay of 8 min, while (b) shows the simulation for a delay of 7 min (with respect to $t = 0$, when feed introduction begins). Operating conditions as in Table 1.

phase composition, obtained by separate isocratic runs). In this context, the agreement between experiment and simulation is reasonable.

Separation of binary feed mixtures

Mixtures of Phe and Trp were used to test the effect of gradient deformation on separation quality. Figure 6 corresponds to a gradient delay of 11 min. Phe has fully eluted under isocratic conditions, while the Trp is found just behind the ACN breakthrough and is therefore concentrated. Reasonable agreement is seen between experiment and simulation.

This run shows how gradient deformation can be used to advantage: the operating conditions were manipulated such that the desired product (Trp) was located just behind the gradient and thereby concentrated, while being separated from Phe.

Discussion

Since peak concentration occurs in the vicinity of the shock layer, the head of the gradient must be modeled accurately for the simulations to give reasonable agreement with experimental results. There are two factors, not accounted for by the present simulations, that could strongly affect gradient deformation. The first is nonideal mixing of ACN and water. This would tend to increase the ACN concentration and thus

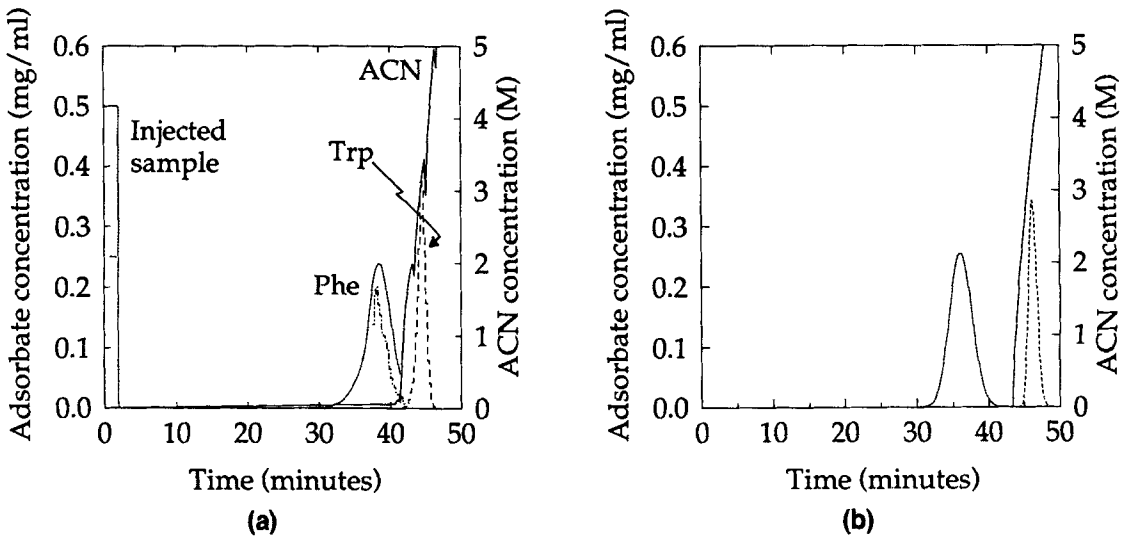

Figure 6. Binary mixture run.

Separation of Phe and Trp under conditions of gradient deformation. Gradient delay of 11 min with respect to $t = 0$. Operating conditions as in Table 1. (a) Shows the experimental result, and (b) the corresponding simulation.

to increase the shock strength. The shock layer would then move faster, which would account for the time difference between Figures 3 and 4. The second factor, which is harder to assess, is the degree of well-mixedness achieved in the gradient former (the part of the gradient delivery system that mixes the ACN and water together in appropriate quantities so as to generate the desired gradient). At the beginning of the process, when the ACN is just introduced into the former, the possibility for error is high; this corresponds to the head of the gradient.

The exact process is therefore difficult to model accurately. Further, small changes in the position or strength of the modulator shock can result in large changes in adsorbate peak shapes (cf. Figures 3–5). For example, if the shock strength were increased by around 5% (for example, due to nonideal mixing of ACN and water), the discrepancy of 2 min between experiment and simulation for the Phe runs in Figure 3 would be removed. The agreement between experiment and theory in Figure 2b, at the head of the gradient, is also not exact, and such small differences could affect the separation appreciably. However, these gradient separations involving shock formation are experimentally reproducible. Once the gradient system has been set up for a given separation, an experienced practitioner can rapidly arrive at the optimum conditions of gradient slope and delay.

In addition, accounting even approximately for nonlinear modulator adsorption can provide better results than the classic theories. El Fallah and Guiochon (1991) have applied our theory of nonlinear modulator adsorption to gradient elution on an octadecyl silica solvent, thereby improving agreement with experiment, even though the operating conditions were such that no shock layer was formed.

Other modes of chromatography

Nonlinear modulator adsorption is not restricted to reversed-phase chromatography, and we briefly discuss its implications for two other commonly used chromatographic techniques: ion-exchange and hydrophobic interaction chromatography.

In hydrophobic interaction chromatography, the salts that are used as modulators usually do not bind strongly to the stationary phase. For example, when ion-exchange adsorbents are used at very high salt levels as hydrophobic-interaction supports, all the electrostatic binding sites on the stationary phase have already been occupied by salt counterions. This is why hydrophobic interactions, which are weaker than electrostatic interactions, become dominant at high salt levels in the first place. Thus the decreasing salt gradient used in hydrophobic interaction does not generally exhibit appreciable adsorption, and the classic theory of unretained modulators is appropriate. Hydrophobic interaction chromatography is also carried out on uncharged sorbents. Again, in the absence of considerable hydrophobic patches on the sorbent, the salt is unable to bind appreciably and the classic theory is appropriate.

Ion exchange chromatography involves the complication of electroneutrality, which requires that the stationary phase always be saturated. If the column is preequilibrated with the same salt (buffer) that is to be used as the modulator, the salt will already have saturated the stationary phase, regardless of its initial concentration. Thus the modulator, when it enters the column in the gradient, cannot adsorb, and will travel as an unretained component. If, on the other hand, the column is initially equilibrated with a buffer salt different from the modulator, the modulator on entering the column will adsorb competitively. In this case, nonlinear modulator adsorption again becomes possible, and so consequently does gradient deformation. These possibilities deserve further study.

Conclusions

The experiments discussed in this article have experimentally verified that nonlinear modulator adsorption gives rise to gradient deformation. The isotherm formalism used worked well in capturing the multicomponent adsorption of acetonitrile and water, as seen by the agreement between theory and experiment in Figure 2a. The single-component runs for Phe showed that unusual behavior occurs when an adsorbate peak is found in the vicinity of the strongly deformed gradient. Both the single-component Phe runs and the binary separation showed that adsorbate peaks can be concentrated, and the binary separation of Trp and Phe exemplified the possibility of simultaneous concentration and separation.

Acknowledgments

This work was supported by NSF grants BCS-8912150 and NASA NSCORT grant NAGW-2329. We thank Kent Hamaker and Subir Basak for their helpful comments during preparation of this manuscript.

Notation

a_M = Langmuir isotherm parameter, mL/g
a^0 = molar surface area, m^2/mol
A_s = specific surface area of sorbent, m^2/g
b_M = Langmuir isotherm parameter, M^{-1}
C = mobile phase concentration, mg/mL
C_{feed} = mobile phase concentration of feed, mg/mL
C_M, C_N = mobile phase concentration of modulator (ACN), M
$C_{N,0}$ = initial mobile phase concentration of modulator (ACN), M
C_p = pore liquid concentration, mg/mL particle
d_p = particle diameter, m
D_M = molecular diffusivity, cm^2/s
D_p = particle diffusivity, cm^2/s
E = axial dispersion coefficient, cm^2/s
f = association factor of water (= 2.6), dimensionless
F = volumetric flow rate, mL/min
k_f = film mass-transfer coefficient, cm/s
k^0 = overall lumped mass-transfer coefficient, s^{-1}
K_{ads} = distribution coefficient (Henry's law constant for adsorption), mL particle void volume/g particle
K_M = Jovanovic isotherm parameter, M^{-1}
K_{vol} = distribution coefficient, mL particle void volume/mL particle solid volume
M_W = molecular weight of water, g/mol
n^s = saturation concentration on the stationary phase, mmol/g
Pe = Peclet number ($= ud_p/D_M$), dimensionless
q = stationary phase concentration, mg/g (Phe and Trp) or mmol/g (ACN)
q^* = equilibrium stationary phase concentration, mg/g (Phe and Trp) or mmol/g (ACN)
q_p = local adsorbed concentration, mg/g particle
r = radial distance into particle, cm
Sh = Sherwood number ($= k_f d_p/D_M$), dimensionless
t = time, s
T = absolute temperature, K

t_{inj} = period of feed injections
t_R = retention time (first moment), s
t_l = number of layers adsorbed to stationary phase, dimensionless
v_{chrom} = chromatographic velocity, cm/s
v_s = molar volume of solute at the normal boiling temperature, cm^3/g-mol
v_{sup} = superficial velocity, cm/s
x = distance into column, m
x^s = adsorbed mole fraction, dimensionless
x^l = mobile phase mole fraction, dimensionless

Greek letters

α = slope of gradients at column inlet, M/min
μ_b = desorption rate constant, s^{-1}
ϵ_b = bulk (interstitial porosity), mL interstitial void volume/mL empty column volume
ϵ_p = intraparticulate porosity, mL particle void volume/mL particle
ρ_p = particle density, g/mL particle
η_w = viscosity of water, cp
$\Gamma^{(n)}$ = area surface excess, mol/m^2
ϕ = phase ratio, g/mL
Λ_M = Jovanovic isotherm parameter, mmol/g
τ = tortuosity of stationary phase, dimensionless
σ^2 = variance (second central moment), s^2

Subscripts

i = ith species
j = jth species
M, N = modulator (ACN)

Literature Cited

Acrivos, A., "Methods of Characteristics Technique," *Ind. Eng. Chem.*, **48**, 703 (1956).

Arnold, G. H., H. W. Blanch, and C. R. Wilke, "Analysis of Affinity Separations: I. Predicting the Performance of Affinity Adsorbers," *Chem. Eng. J.*, **30**, B9 (1985a).

Arnold, F. H., H. W. Blanch, and C. R. Wilke, "Analysis of Affinity Separations: II. The Characterization of Affinity Columns by Pulse Techniques," *Chem. Eng. J.*, **30**, B25 (1985b).

Conway, B. E., *Electrochemical Data*, Elsevier, Amsterdam (1952).

Courant, R., and D. Hilbert, *Methods of Mathematical Physics: II. Partial Differential Equations*, Interscience, New York (1962).

Danckwerts, P. V., "Continuous Flow Systems. Distribution of Residence Times," *Chem. Eng. Sci.*, **2**, 1 (1953).

DeVault, D., "The Theory of Chromatography," *J. Amer. Chem. Soc.*, **65**, 532 (1943).

Durão, M. I. G., C. A. V. Costa, and A. E. Rodrigues, "Saturation and Regeneration of Ion-exchangers with Volume Changes," *Ind. Eng. Chem. Res.*., **31**, 2564 (1992).

El Fallah, M. Z., and G. Guiochon, "Gradient Elution Chromatography at Very High Column Loading: Effect of the Deviation from the Langmuir Model on the Band Profile of a Single Component," *Anal. Chem.*, **63**, 2244 (1991).

Emmett, P. H., and S. Brunauer, "The Use of Low Temperature van der Waals Adsorption Isotherms in Determining the Surface Area of Iron Synthetic Ammonia Catalysts," *J. Amer. Chem. Soc.*, **59**, 1553 (1937).

Everett, D. H., "Thermodynamics of Interfacial Phenomena," *Pure Appl. Chem.*, **53**, 2181 (1981).

Furusawa, T., M. Suzuki, and J. M. Smith, "Rate Parameters in Heterogeneous Catalysis by Pulse Techniques," *Catal. Rev. Sci. Eng.*, **13**, 43 (1976).

Helfferich, F., and G. Klein, *Multicomponent Chromatography. Theory of Interference*, Marcel Dekker, New York (1970).

Jandera, P., and J. Churacek, *Gradient Elution in Column Liquid Chromatography. Theory and Practice*, Elsevier, Amsterdam (1985).

Kipling, J. J., and D. A. Tester, "Adsorption from Binary Mixtures: Determination of Individual Adsorption Isotherms," *J. Chem. Soc.*, **52**, 4123 (1952).

Koch, C. S., F. Köster, and G. H. Findenegg, "Adsorption of Binary Solvent Mixtures in Reversed-phase Chromatographic Systems. Surface Excess Isotherms and Enthalpies of Displacement," *J. Chromatog.*, **406**, 257 (1987).

LeHa, N., J. Ungvaral, and E. sz. Kováts, "Adsorption Isotherms at the Liquid-Solid Interface and the Interpretation of Chromatographic Data," *Anal. Chem.*, **54**, 2410 (1982).

Lin, J. K., B. J. Jacobson, A. N. Pereira, and M. R. Ladisch, "Liquid Chromatography of Carbohydrate Monomers and Oligomers," *Methods Enzymol.*, **160**, 145 (1988).

Marra, R. A., and D. O. Cooney, "Multicomponent Sorption Operations: Bed Shrinking and Swelling in an Ion-Exclusion Case," *Chem. Eng. Sci.*, **33**, 1597 (1978).

Rusanov, A. I., in *Progress in Surface and Membrane Science*, Vol. 4, Academic Press, New York, p. 57 (1967).

Ruthven, D. M., *Principles of Adsorption and Adsorption Processes*, Wiley, New York (1984).

Satterfield, C. N., *Mass Transfer in Heterogeneous Catalysis*, MIT Press, Cambridge, MA (1969).

Schay, G., and L. Nagy, "Nouveaux Aspects de l'Interprétation des Isothermes d'Adsorption de Mélanges Liquides Binaires sur des Surfaces Solides," *J. Chim. Phys.*, **58**, 149 (1961).

Schneider, P., and J. M. Smith, "Adsorption Rate Constants from Chromatography," *AIChE J.*, **14**, 762 (1968).

Slaats, E. H., W. Markovski, J. Fekete, and H. Poppe, "Distribution Equilibria of Solvent Components in Reversed-Phase Liquid Chromatographic Columns and Relationship with the Mobile Phase Volume," *J. Chromatog.*, **207**, 299 (1981).

Snyder, L. R., and M. A. Stadalius, in *High-Performance Liquid Chromatography, Advances and Perspectives*, Vol. 4, Cs. Horváth, ed., Academic Press, New York, p. 195 (1986).

Snyder, L. R., in *High-Performance Liquid Chromatography, Advances and Perspectives*, Vol. 1, Cs. Horváth, ed., Academic Press, New York (1980).

Tani, K., and Y. Suzaki, "Comparison of the Isotherms for Monomeric and Polymeric C-18 Bonded Stationary Phases," *J. Chromatog. Sci.*, **27**, 698 (1989).

Velayudhan, A., and M. R. Ladisch, "Role of the Modulator in Gradient Elution Chromatography," *Anal. Chem.*, **63**, 2028 (1991).

Velayudhan, A., and M. R. Ladisch, "Effect of Modulator Sorption in Gradient Elution Chromatography: Gradient Deformation," *Chem. Eng. Sci.*, **47**, 233 (1992).

Velayudhan, A., and M. R. Ladisch, in *Bioproducts and Bioprocesses* 2, T. Yoshida and R. D. Tanner, eds., Springer-Verlag, Berlin, p. 217 (1993).

Wilson, E. J., and C. J. Geankoplis, "Liquid Mass Transfer at Very Low Peclet Numbers in Packed Beds," *Ind. Eng. Chem. Fundam.*, **5**, 9 (1966).

Yamamoto, S., K. Nakanishi, and R. Matsuro, *Ion-Exchange Chromatography of Proteins*, Marcel Dekker, New York (1988).

Manuscript received Feb. 24, 1994, and revision received Aug. 1, 1994.